

Operational modal analysis and FE model updating of the Metropolitan Cathedral of Santiago, Chile



Wilson Torres^a, José Luis Almazán^a, Cristián Sandoval^{a,b,*}, Rubén Boroschek^c

^a Department of Structural and Geotechnical Engineering, Pontificia Universidad Católica de Chile, Vicuña Mackenna 4860, Santiago de Chile, Chile

^b School of Architecture, Pontificia Universidad Católica de Chile, Casilla 306, Correo 22, Santiago de Chile, Chile

^c Department of Civil Engineering, University of Chile, Beauchef 850, Santiago de Chile, Chile

ARTICLE INFO

Article history:

Received 21 August 2016

Revised 6 February 2017

Accepted 5 April 2017

Available online 20 April 2017

Keywords:

Monumental structures
Operational modal analysis
Finite element model
Model updating
Stone masonry

ABSTRACT

Heritage buildings in Latin American countries possess high architectural value. Studying these constructions under extreme loads, particularly earthquakes, requires representative models for simulating expected response. At present, the non-invasive Operational Modal Analysis (OMA) tests offer interesting possibilities for obtaining modal parameters to update and validate a structural model for this type of structure. In this context, this article focuses on the calibration and adjustment process for a finite element model of the Metropolitan Cathedral of Santiago Chile, based on experimentally identified modal and mechanical material properties. Accordingly, an in situ experimental campaign, aimed at obtaining the response of the structure due to ambient vibrations is presented and discussed. Six high-sensitivity synchronous triaxial accelerometers were employed in this campaign. Enhanced Frequency Domain Decomposition (EFDD) and Stochastic Subspace Identification (SSI), system identification methods, were applied. Mechanical tests were performed on the Cathedral's stone blocks. The experimental data and derived modal properties were used to generate and update a finite element model. Several considerations were made in the model updating process: the most relevant was the homogeneous treatment of the stone masonry with their mortar interface, and the boundary elements restraining effect caused by adjacent structures. A preliminary model updating process was applied to define the boundary conditions and initial material properties. This optimization was based on minimizing an error function given by the difference between the experimental and analytical frequencies. A second step was then applied, in which models with different material properties were evaluated within a physically possible range. The final model selection was based on the distance between the experimental and analytical frequencies, and the mode shapes. The updated model allows an assessment to be made of the structure behavior in its current condition and models to be prepared for a wide range of possible future research scenarios.

© 2017 Elsevier Ltd. All rights reserved.

1. Introduction

Studying the structural performance of heritage masonry constructions has become a priority in cities around the world where architectural heritage needs to be preserved. However, this assessment remains a complex task. A major difficulty is knowing the mechanical properties of component materials, the current structural damage, and the degree of interaction between various internal and external elements and systems. Because of these and other difficulties, some general recommendations for structural analysis

of historic constructions have been proposed using a multidisciplinary approach [25].

Powerful computational tools are currently available for assessing the structural behavior of historic masonry construction. A summary of the different available strategies can be found in Roca et al. [44]. Analytical models of these structures can be from detailed models, like micro-modeling [30] or simplified models that consider the masonry as a continuous isotropic material [39]. In the latter modeling type, the yield surface for compression is given by the Hill criterion and the yield surface for traction by the Rankine criterion [17]. This approach is more manageable, because it has adequate computational effort, fewer parameters and a mathematically simpler representation [44].

A methodological approach to assessing a historic building should incorporate non-destructive or minimally destructive

* Corresponding author at: Department of Structural and Geotechnical Engineering, Pontificia Universidad Católica de Chile, Vicuña Mackenna 4860, Santiago de Chile, Chile.

E-mail address: csandoval@ing.puc.cl (C. Sandoval).

Nomenclature

a_i, b_i, c_i	Quadratic function constants for i th frequency	ϕ_{exC}	Experimental complex mode
d	Distance between experimental and numerical model	ϕ_{exR}	Equivalent real mode to the experimental complex mode
E	Young's module	ϕ_{ex_i}	i th experimental modal shape
$E_{30-60\%}$	Young's module, experimentally determined in the monotonic compression test, in the range 30% to 60% of the maximum strength	ϕ_i	i th numerical modal shape
E_{bm}	Young's modulus of brick masonry	$()^T$	Transposed matrix
E_{rm}	Young's modulus of reinforced brick masonry	$()^{-1}$	Inverse matrix
E_{sm}	Young's modulus of stone masonry	CTE10	Quadratic tetrahedral element of 10 nodes
f_c	Compressive strength	DD	Damage in dome
f_{ex_i}	i th frequency obtained from experimental model	DLW	Damage in central longitudinal wall
f_i	i th frequency obtained from numerical model	DTA	Damage in transverse arch
$Im(*)$	Imaginary part of the complex mode	EFDD	Enhanced Frequency Domain Decomposition
J	Minimizing function in the model update process	FDD	Frequency Domain Decomposition
$Re(*)$	Real part of the complex mode	FMAC	Frequency scaled MAC
w_i	i th weighting factor for each i th frequency	GPS	Global Positioning System
w_f	Weighting factor for frequency term	MAC	Modal Assurance Criterion
$w_{i,MAC}$	i th weighting factor based on the MAC between experimental modal shape and numerical one	OMA	Operational Modal Analysis
w_ϕ	Weighting factor for modal shape term	SA	Setup located on base of arches
x_j	j th calibration parameter for the model updating process	SSI	Stochastic Subspace Identification
ϵ_i	Error between experimental and numerical frequency	ST	Setup located on top of walls
		SW	Setup located on base of windows
		UTC	Coordinated Universal Time

experimental techniques. One example is the well-known vibration analysis technique, used to estimate the structure's natural frequencies and modal shapes. The modal parameters thus obtained can then be used to calibrate numerical models by adjusting their mechanical properties [5]. Among the non-invasive methods the Operational Modal Analysis (OMA) is the most commonly used [4,15,42]. By measuring the response to ambient vibrations and assuming that the input is white noise, the modal properties can be defined based on the system identification process. There are some complications involved in using OMA methodology, including: signal noise from the very long cables [18], the difficulty of detecting modal shapes for very close modes, definition of adequate system order (in case of parametric identification method), and detection of spurious modes generated by signal noise [33].

Several studies have used OMA methodology with the aim of studying the components of historical constructions, mainly towers, vaults, domes and arches [9,21]. By contrast, defining the modal properties in a historic structure's more rigid zones, like perimeter walls and resistant transverse and longitudinal axes, is a less studied subject. One of the main difficulties relates to the complexity of identifying high-frequency close modes, which are common in structures with uniform stiffness and mass distribution. Additionally, the low-response level to ambient excitation and the typical device resolution and precision make their identification a confusing and difficult process [12,13].

One additional difficulty in identifying structural systems in this type of structures is that their structural elements do not have purely flexural or torsional modes, but a mixture of the two, unlike what occurs in conventional structures [10]. Therefore, the measuring devices need to be distributed in the structure, to capture all these special movements. Another common difficulty relates to the highly nonlinear response, which is due to the friction interaction between units at low deformation levels; this introduces anomalies, which can be confused with structure modes, i.e. they generate spurious vibration modes that can cause interpretation problems in the identification process [12].

In similar previously developed cases, preliminary analytical models were developed, from which an optimal location for the

response measuring devices was defined [32] based on the modes to be identified. Although this analysis is a good initial guide for defining the location of measuring points, the final location will depend on the structure's accessibility and operational conditions for measuring its response to environmental vibration.

Within the identification process, there is a list of previous research in which a frequency domain method (FDD) is contrasted with a time domain method (SSI), as making a comparison is important for highly uncertain problems, in order to generate consistent results [18,31,43]. However, there is other research into heritage structure, in which the FDD method alone is enough to identify the structure's mechanical properties [3,20,29]. One of the final aims of some similar studies [1,21,42] is to determine the structures' modal properties using the OMA methodology and subsequently update the model with multivariable optimization techniques [14]. These techniques minimize error function, where the calibration parameters (model variables that can vary within a range) comply with user-given constraints. This error function is given by the difference of the natural frequencies and the structure's modal shapes, between the experimental and analytical model [8].

Chile is widely recognized as one of the most seismic countries in the world. This is due to its location in the subduction zone between the Nazca plate and the South American plate. There are additional seismic considerations for Santiago, the capital city, since there exist two more seismic sources: an intraplate seismogenic source for medium depth earthquakes, and a crustal seismogenic source for superficial earthquakes [28]. An iconic architectural heritage structure of Santiago Chile, is the Metropolitan Cathedral. This historical structure more than 250 years old was chosen as a case study for this research.

The Metropolitan Cathedral of Santiago, Chile, has been affected by environmental factors throughout its history, but mainly by earthquakes occurring on the site [24]. A preliminary research project took place to identify and update the models for the Cathedral [48]. In this research, a mathematical optimization technique was used by minimizing an error function [14] in the model updating process, using only the modal frequency.

The methodology used in this article is as follows: i) Develop an analytical model of the main Cathedral structure, ii) An experimental campaign where the response is recorded by synchronized velocity meters at selected points in the structure, iii) Processing the signals obtained in the experimental campaign, iv) Modal identification of the structural system, v) Compression tests on rock samples from the structure, vi) Initial adjustment of mechanical properties by solving an optimization problem using only modal frequency, vii) Develop a grid search with models with different mechanical properties. After this introductory section, the article is organized as follows: ii) Overview of the Cathedral; iii) Analysis of ambient vibrations (OMA); iv) FE models and Model Updating; v) Brief discussion and suggestions; and vi) Conclusions.

2. The metropolitan cathedral of Santiago

2.1. General description

The Metropolitan Cathedral of Santiago is probably the most important historical structure in Chile's capital city. It is east-west oriented and is located in the northern center of the city. Its construction dates back to 1746 and its architectural style is neo-classical. It has a length of 110 m and a width of 30 m, with three longitudinal naves (Fig. 1).

The structural system consists mainly of stone masonry walls up to a height of 11 m and then brick masonry walls to a height of 17 m. The roof structure consists of wooden trusses in the center and north naves, while the south nave has metal trusses. Two bell towers of 45 m height can be distinguished in the main façade (Fig. 2a). These structures are composed of steel columns at the corners, covered by brick masonry. The central nave is the highest (Fig. 2b), with a ridge height of 20 m, while the lateral naves are 15 m high. On the central nave, between the 10–11 and B–C axes (Fig. 1), there is the main 50 m high dome. The dome base is composed of steel beams, which support the brick masonry walls cre-

ating its outline. On top of this dome, there is a three-dimensional lattice structure supporting the roof.

2.2. History of construction

Before the Cathedral that exists today, the original structure had a south-north orientation. This structure was planned and built between 1544 and 1570 [41]. Several earthquakes have hit the Cathedral over its history, and in 1769 was almost completely destroyed by fire. In 1746, years before its complete destruction, the Bishop at the time decided to build a new cathedral, which is the basis of the present building. The construction of the new Cathedral began in 1748; the two Cathedrals coexisted in the same place up to 1769, with the old structure oriented perpendicularly to the new one.

Based on experience with the first structure, it was concluded that the new Cathedral should have buttresses to provide more lateral resistance; stone blocks, instead of adobe, were determined to be the base material of the new structure. Construction proceeded from the western toward the eastern facade, but after the death of the chief architect, a new builder took charge of the project in 1770. In 1830, the first stage of the construction ended, without towers nor the dome. Construction of the chapel started in 1846, later stopped and then resumed in 1858. Additionally, the first tower was built, but it did not correspond to any existing tower in the current Cathedral.

Subsequently, two earthquakes occurred in Santiago, one in 1851 and another in 1874. Severe damage was generated by the first one in most of central nave arches; only the first and tenth arches from the western facade have no damage. The damage was repaired in 1854. The 1874 earthquake affected the 3 main arches of the eastern facade. The Bishop ordered the remodeling of the Cathedral in 1897, which included two towers on the main facade, the dome above the altar, the roof, the removal of intermediate pilasters supporting the choir, and other architectural remodel-

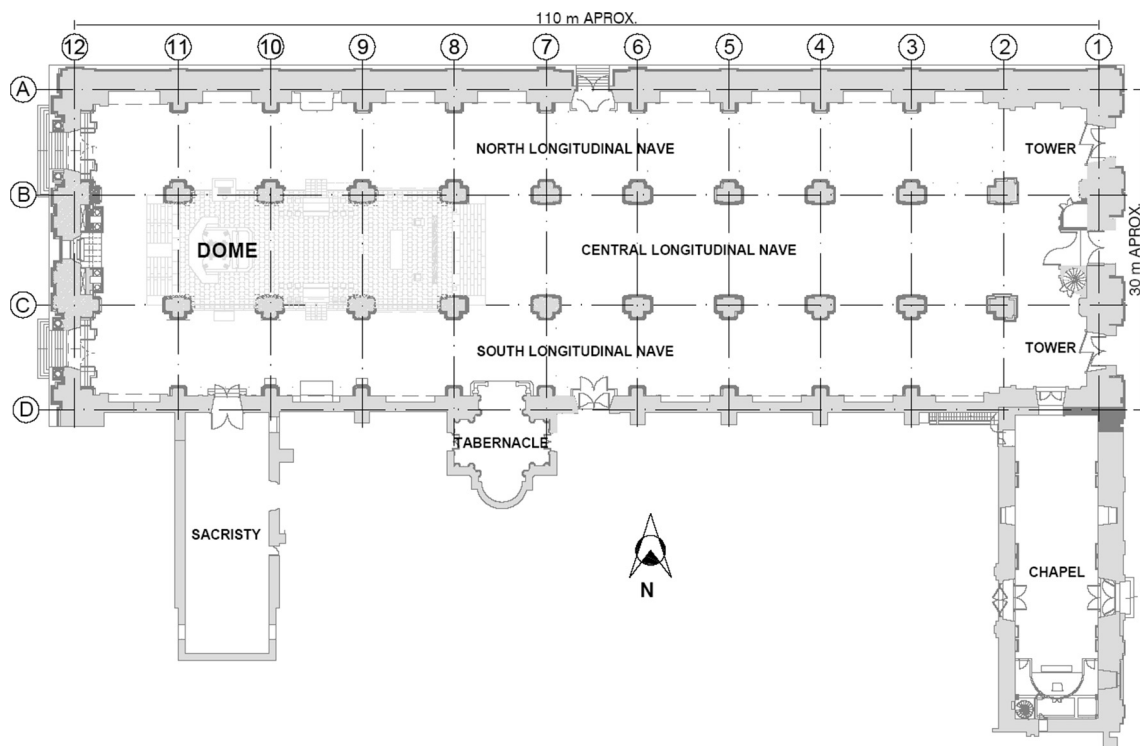


Fig. 1. General plan view of the Metropolitan Cathedral of Santiago, Chile.



Fig. 2. Metropolitan Cathedral of Santiago, Chile: a) Main façade, b) View of the central nave.

eling. The tower was demolished in 1898, and the rest of the works were completed by 1906 [24].

The Metropolitan Cathedral of Santiago was declared a National Historic Monument in 1951, and another major remodeling took place on the cathedral, specifically the archbishop's crypt in 2006. Thanks to this work, many stones could be obtained that have the same quality as the walls, because they were extracted from the structure base.

2.3. Historical seismic behavior and the current state

The main cause of the Cathedral's damage is the numerous earthquakes that have affected the structure over its lifetime. The March 3rd, 1985 earthquake (Mw 8.0 - Valparaiso) affected both the Cathedral structure and cladding. This led to a repair process of the most significant structural damage, which began in 1999 [40]. Serious but eventually recoverable damages were observed in the Cathedral after the 2010 Maule earthquake.

After the February 27, 2010 earthquake (Mw 8.8 - Maule), the following Cathedral damage was identified as part of this study (DD – Damage in dome, DLW – Damage in longitudinal wall, DTA – Damage in transverse arches):

- DD1: Cracking at the dome base and reinforcing buttress head (Fig. 3).
- DD2: Shear cracks in brick masonry walls that make up the dome (Fig. 4).
- DLW1: Vertical cracks at the junction of central longitudinal walls on the western façade (Fig. 5).
- DLW2: Vertical cracks at the junction of central longitudinal walls with transversal axis 2 wall (Fig. 6).

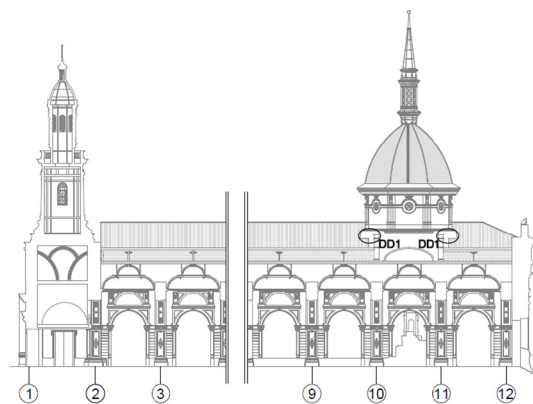


Fig. 3. Cracking at the base of the dome.

- DLW3: Punching cracks in all the pillar heads that support the brick masonry portion in the central longitudinal walls (Fig. 7).
- DLW4: Slippage between the upper brick masonry and stone masonry of the longitudinal walls of the nave, axes B and C (Fig. 8).
- DLW5: Cracks in the upper window of B axis between axes 11 and 12 (Fig. 9).
- DTA1: Cracks in the internal transversal arches, some axes (Fig. 10).

The Metropolitan Cathedral of Santiago de Chile's current damage status does not compromise its overall stability, but could affect the local stability of certain elements in a potential seismic event [24]. On the other hand, due to the massive structure, all these fissures detected in the structure most probably do not work against the low intensity of the ambient vibration. Therefore, even though it is important to define the current damage in the structure, the numerical model of the structure is considered as continuous, as will be mentioned later in the model assumptions.

3. Ambient vibration analysis

An experimental campaign was designed and implemented to estimate the modal properties of the Metropolitan Cathedral of Santiago Chile. A description of the campaign and its main results are presented in this section.

3.1. Experimental campaign

The experimental campaign consists of measuring the response of the structure to ambient vibrations at selected points. To select

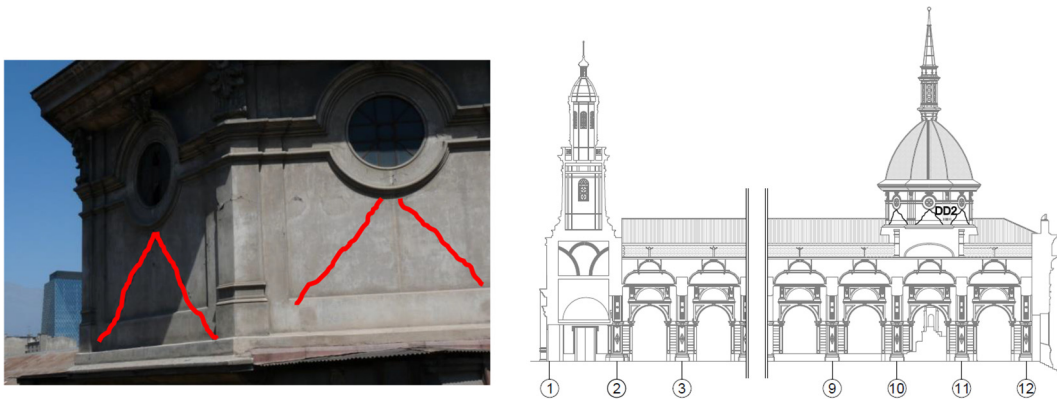


Fig. 4. Cracking at the dome.

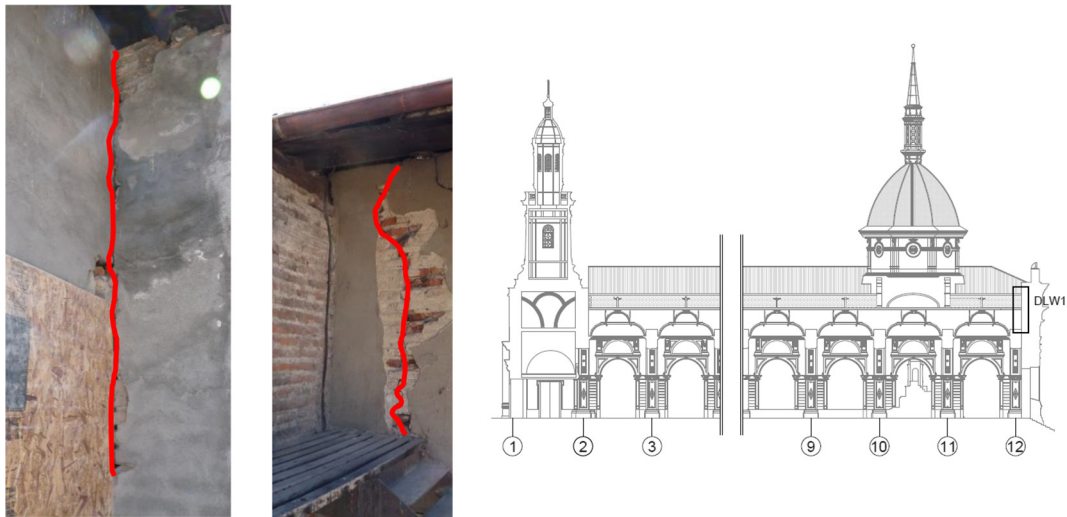


Fig. 5. Cracking at the junction between the central longitudinal axis and the western facade.

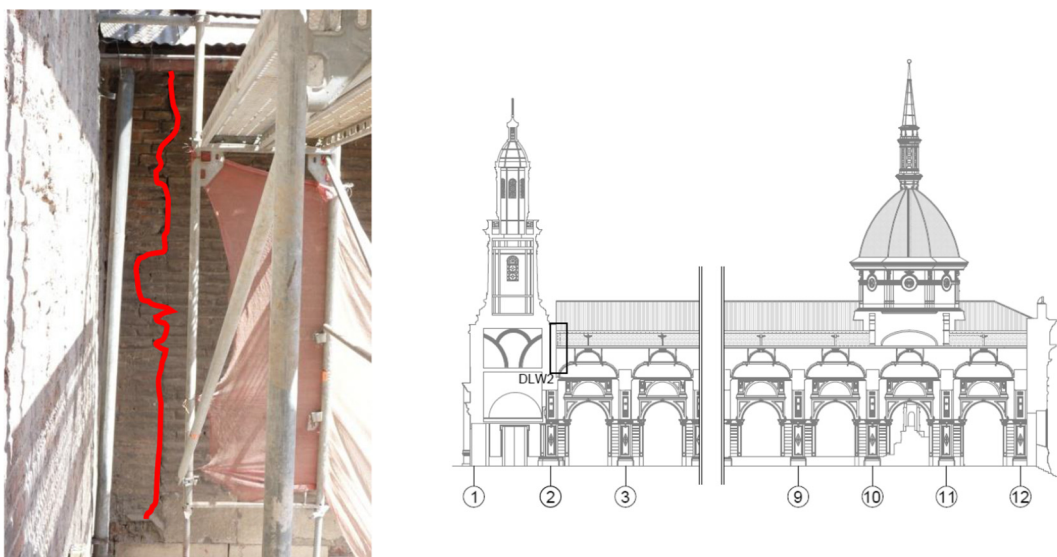


Fig. 6. Cracking at the junction between the central longitudinal axis and the tower base.

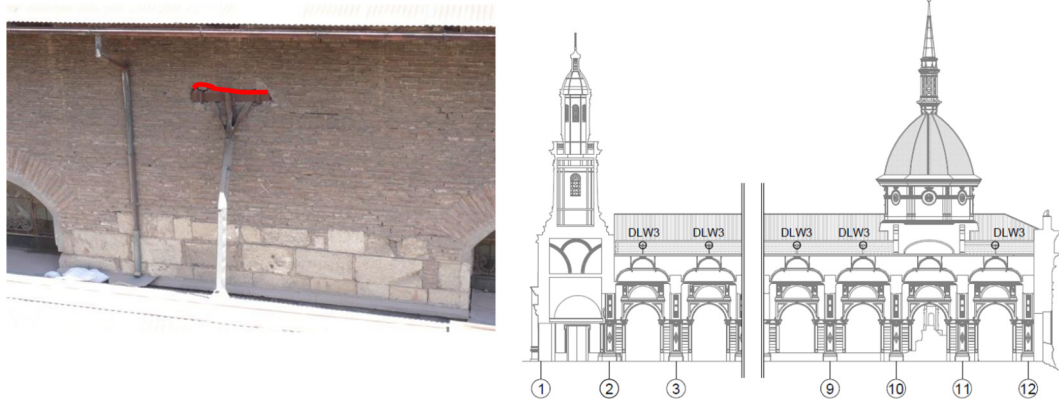


Fig. 7. Steel shoring punching on the masonry.

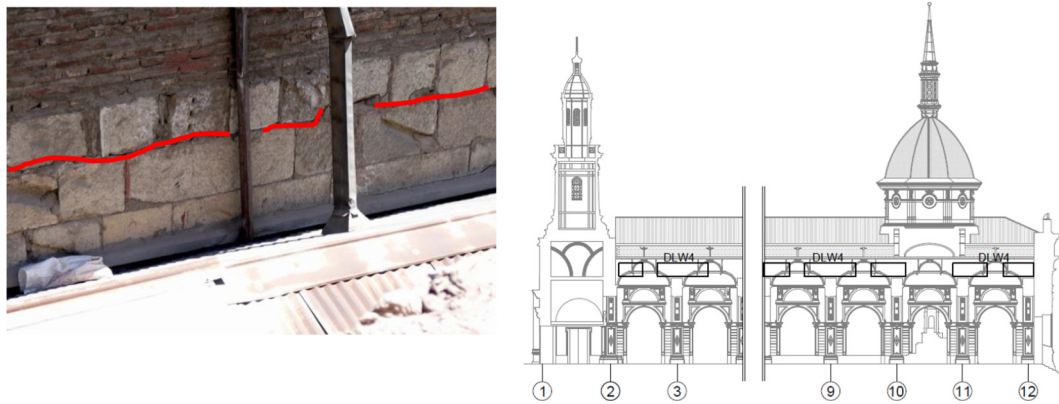


Fig. 8. Cracking at the junction of brick masonry and stone masonry.



Fig. 9. Window of B axis between axes 11 and 12.

these points, areas were first selected where the fundamental modes of a preliminary numerical model possessed higher amplitudes, and then the most easily accessible points were chosen.

Six Trominos devices [36], which measure accelerations and velocity in 3 orthogonal directions, were used during the experimental campaign. The sensor clock was adjusted using UTC time, obtained from a GPS device. This time set-up allows for equipment and signal synchronization. Structure vibration was recorded by measuring velocity, due to its larger signal-to-noise ratio.

Twenty-two set-ups were defined to cover the entire structure; locations are shown in Fig. 11. A set-up is an array of instruments

where the structure response is recorded for at least 20 min; this is consistent with an empirical rule given by Rodriguez [45], where the measurement duration is recommended to be at least 2000 times the natural period of interest, e.g. if this structure begins with a natural frequency of approximately 2 Hz, the measurement duration should be at least 17 min. Two reference instruments, always located at the same position, were used in all set-ups (called REF 1 and REF 2 in Fig. 11). A sampling rate of 128 Hz was used. It is important to note that the instruments were located at different heights, as can be seen in Figs. 12 and 13. To facilitate interpretation of its location a description was defined as follows:

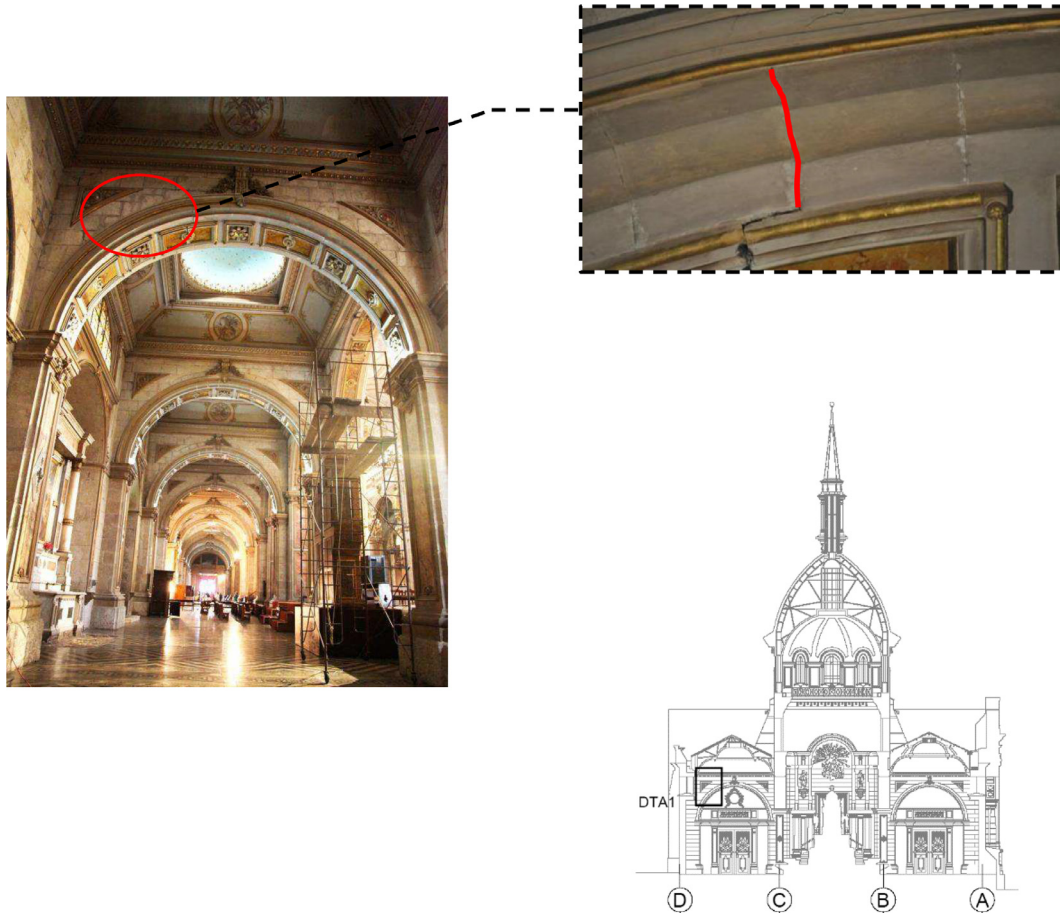


Fig. 10. Cracks in the internal transversal arches.

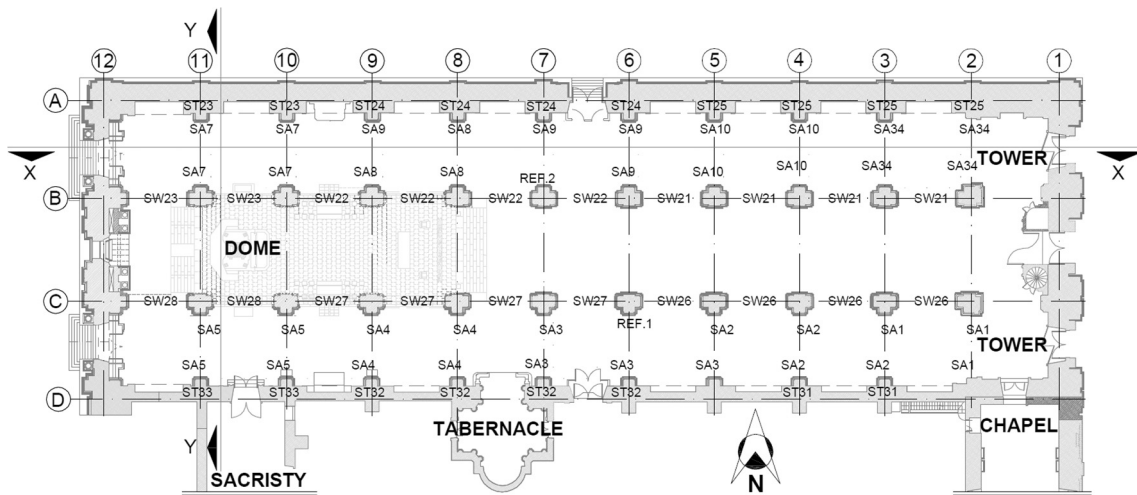


Fig. 11. Location of setups defined in the experimental campaign.

SA: Bases of the arches in the north and south longitudinal naves. This was the location of the reference instruments (C6 and B7 axes).

ST: Top of south and north longitudinal walls.

SW: Window bases of the central longitudinal walls (B and C axes).

Reinforcements were being installed in the Cathedral during the measurements, so some areas were inaccessible. This affected the measurements in the main facade towers and the dome located

above the altar. Another inaccessible area was the inside western wall. Fig. 14 shows the sensor location in the experimental model defined by the ARTEMIS identification software [46] of the main Cathedral structure.

3.2. Signals processing and system identification

Fig. 15a shows the measured velocity records at the reference position (see Fig. 11 – position REF2). Note that the amplitude of

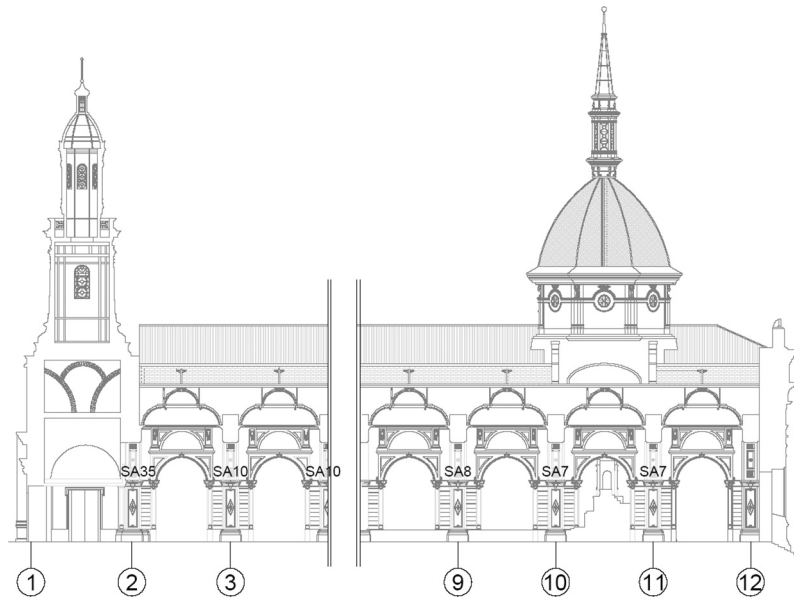


Fig. 12. Section X-X according to plan in Fig. 11, with location of set-ups.

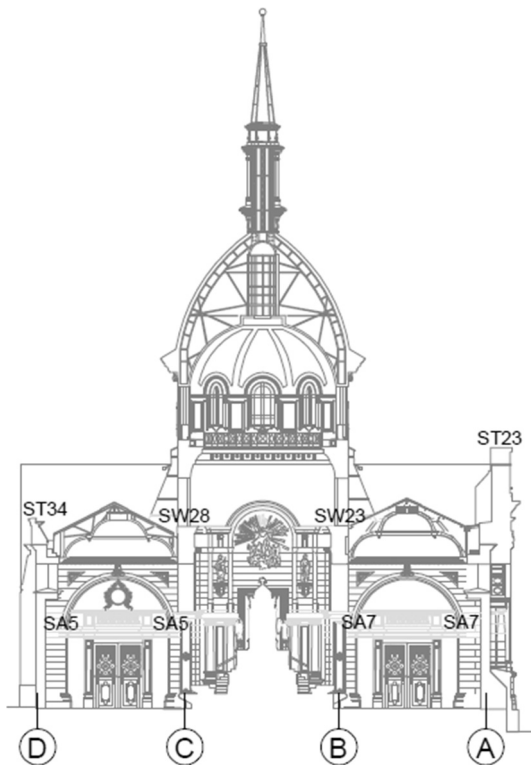


Fig. 13. Section Y-Y according to plan in Fig. 11, with location of set-ups.

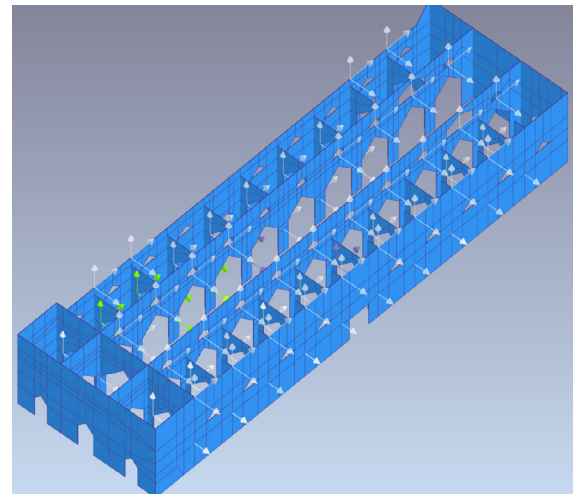


Fig. 14. Artemis model of the Cathedral with localization of sensors.

the recorded movement is very low (about $4.0E - 5$ m/s), which is a characteristic response to ambient vibration in rigid structures. Additionally, Fig. 15b shows the Fourier spectrum for the corresponding signals. This indicates that the recorded structure signals include detectable predominant frequencies in their response.

The signal conditioning consisted of a three-step process: an initial series de-trending, then low-pass filtering with cutoff 8 Hz frequencies, and finally a decimation process in a band between 0 and 8 Hz. This whole process generated signals for further processing the structural system identification.

Two different OMA methods were used in this research: EFDD [6] and SSI [51]. As the name implies, the first method is an improved version of the FDD method (Frequency Domain Decomposition) [7]. These improvements consist mainly of determining frequencies and damping by the correlation function, and determining the mode shape by the weighted sum of the singular vector decomposition. The EFDD method was applied using a manual peak-picking process on the singular value curves. On the other hand, the SSI method was applied based on Crystal Clear algorithm [23] and stabilization diagrams for the visualization of results.

Fig. 16 shows the singular values of the spectral densities for two cases: Fig. 16a is the average singular value for all setups, and Fig. 16b is the singular values graph of setup #10 that shows the peaks not clearly visible in Fig. 16a. The potential EFDD frequencies were first selected by peak picking process to evaluate the experimental mode validities, the frequency selection was then confirmed by SSI method. Fig. 17 shows the stabilization diagrams for two setups (13 and 8), in which the frequencies obtained confirm the modes obtained from the EFDD method. Finally, the linear

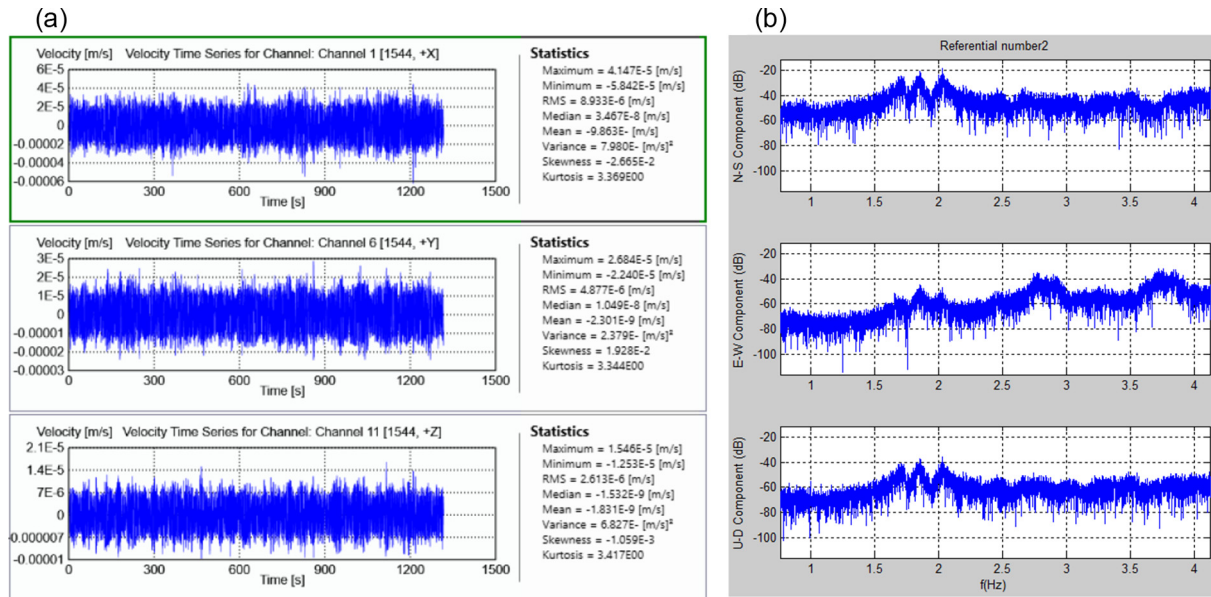


Fig. 15. Velocity signals of a second reference point in setup 1 a) Time series. b) Fourier spectrum of the time series.

independence of these experimental modes was verified from the calculus of Modal Assurance Criterion (MAC) [2] between them.

Fig. 18 shows the MAC between experimental modes. The final experimental modes used in the model updating process will be based on a visual comparison between experimental and analytical mode shapes, and their MAC calculation.

Therefore, the defined experimental modes, based on the identification methods, can be seen on Table 1. For all experimental mode pairs observed in Table 1, the frequencies defined according to EFDD are very close to SSI frequencies. The differences between frequencies are because the frequency values identified correspond to a band and not to precise values, given the non-linearity in the behavior of the structure.

3.3. Determination of mechanical properties of materials

Following the procedure proposed by Oliveira [38], 3-cylinders, 12 cm high and 5 cm in diameter were extracted from an intact rock block used in the structure. The samples were subjected to monotonic compression testing; the results are shown in Table 2. Additionally, a value of 2400 kg/m³ was experimentally determined for the stone density.

According to Table 2, the average value of Young's modulus obtained in the 30% to 60% range of maximum strength was 13,900 MPa, and the average compressive strength value was 111 MPa. These values can be associated with a high quality limestone [35].

The elasticity modulus required for the computational model should consider the entire wall behavior of this material, as well as joints. The investigations of Oliveira [38] and Lourenço [30] show that the Young's modulus for cores obtained from stone is much higher than from block and mortar wall. This is not surprising: in the field of rock mechanics, an intact rock modulus is well known to be up to 10 times greater than the cracked solid modulus [22]. So, the joints between blocks were assumed to behave like cracks in a (pseudo) rock mass, and an initial Young's modulus of stone masonry was adopted to the order of one tenth of the value obtained in the intact specimen test, i.e. 1390 MPa. The assumed value of Young's modulus is consistent with that of roughhewn stone masonry suggested by Italian Code for Constructions [26], where the Young's modulus is between 1020 and 1440 MPa.

In the case of brick masonry located on top of the stone masonry, it was not possible to obtain representative material for a compressive test. Therefore, an experimental value obtained by Villedor et al. [50] from another heritage building located close to the Cathedral and contemporaneously built, coinciding with the finishing of the walls in height and the growth of the Cathedral central nave at the end of the 19th century, is used as the first proposed value. Consequently, an initial value of the Young's modulus of 1780 MPa and a density of 1800 kg/m³ were defined for brick masonry. It should be note that the assumed Young's modulus is within the range of reference values (1200–1800 MPa) for brickwork suggested by the above-mentioned building code (Italian Code for Construction NTC08, 2008). The top of the north façade of Cathedral is reinforced with metal anchors; which is why there is a third material, called reinforced brick masonry, whose modulus is initially assumed to be at the same brick masonry value. Table 3 summarizes the initial values for calibration parameters.

As mentioned above, once the structure's modal properties were identified, the Finite Element (FE) model was updated by adjusting the mechanical properties of materials making up the structure.

4. Finite element analysis and model updating

This section first describes the finite element model, then the mechanical properties are defined using a two-stage optimization problem. The first adjustment of mechanical properties and boundary conditions, given by adjacent structures, was based on minimizing the error function between experimental and analytical frequencies. A second stage of model updating process was carried out, based on minimizing the difference between frequency and MAC values, when varying the Young's moduli of the three main materials within physically ranges. So, the research will compare the results obtained by the two stages of model updating.

Some assumptions are made as a basis for the model. Firstly, the structure's behavior is considered as continuous, without discontinuities in the wall intersections. Secondly, the structure's flexible components (towers and dome) have been represented as simple elements, because the rigid part of the structure is the focus. Thirdly, the adjacent structures (sacristy, tabernacle and chapel)

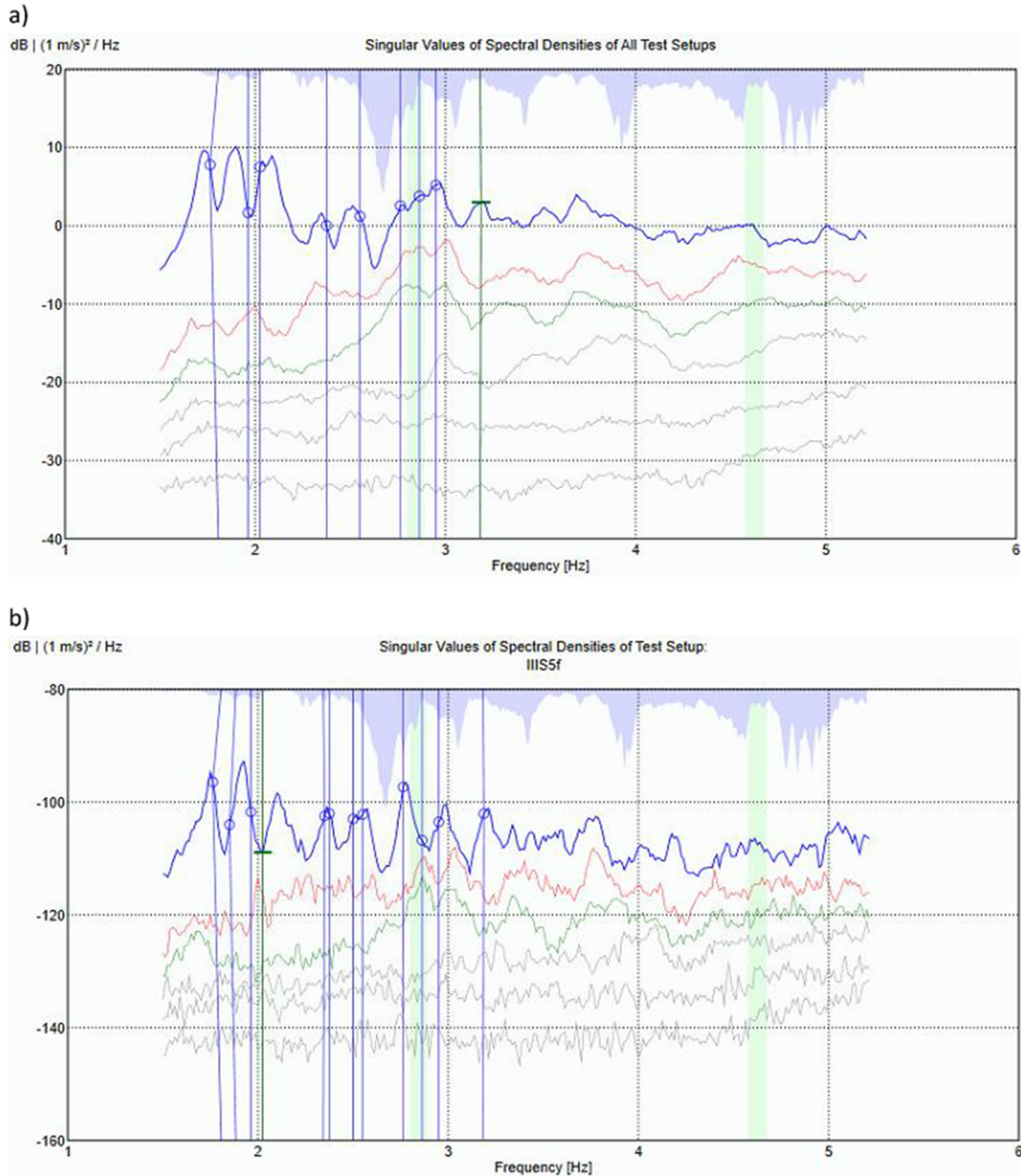


Fig. 16. Singular values of the spectral densities marking natural frequencies by manual peak peaking process in: a) Average of singular values of Spectral Densities for all test setups. b) Singular values of Spectral Densities for test setup 10.

that interact with the principal Cathedral structure can be represented as elastic elements, to simplify the principal Cathedral structure. Finally, mechanical material properties of the structure can be characterized as representative values for the whole structure, disregarding the high variability of these properties in different structural zones.

4.1. Model description

Given the model's complexity and size, the mesh had been previously generated with GID software [11]. The structure's computer model was analyzed using the DIANA software [47].

The finite element model includes detailed modeling of the structure's rigid area and simplified modeling of the towers and

dome, using concentrated masses connected by frame elements with flexo-compression capacity. Additionally, the effect of the adjacent structures (chapel, tabernacle and sacristy, as seen on Fig. 1) is represented by elastic elements that generate lateral interaction with the structure. This way of representing the adjacent structures is used because each one was built at different times [24,40]. This leads to the conclusion that if the model included all adjacent structures, additional parameters and uncertainty would increase, which in turn would increase the difficulty of optimization. The soil type in the area is high quality gravel [49], and so the base nodes are considered to be fully restricted.

The model is built mainly with quadratic tetrahedral elements of 10 nodes (CTE10) with 3 degrees of freedom (translational) per node. The quadratic property of the elements contributes

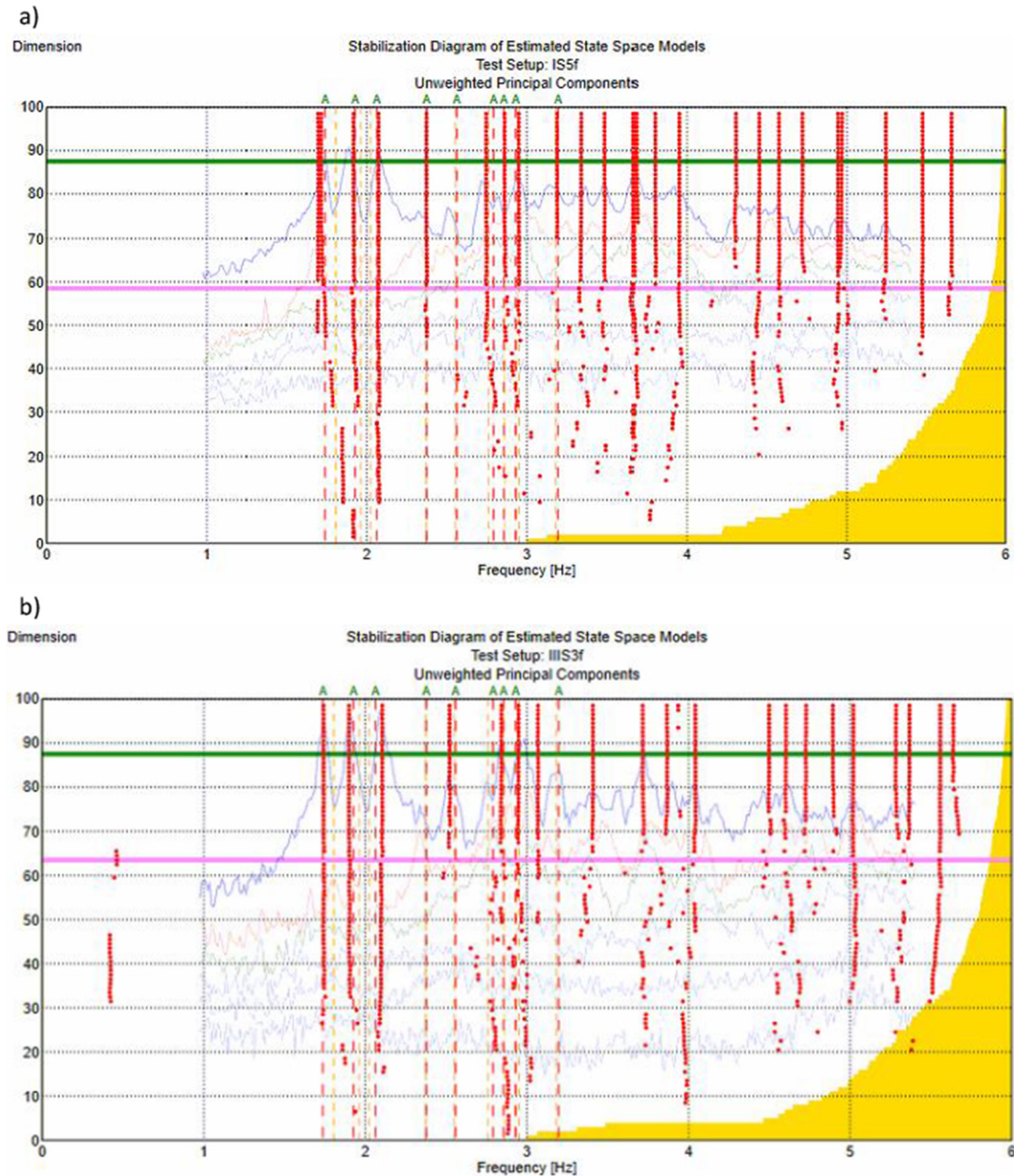


Fig. 17. Stabilization diagrams to define stable modes for two particular setups: a) Setup 13, b) Setup 8.

greatly to convergence in obtaining the natural frequencies model. The complete model has 271,106 nodes, 5195 of which are fully restricted at the base. Therefore, there are 797,733 degrees of freedom. There are 153,992 CTE10 elements, 3038 frame elements to represent flexible zones of the structure; and 450 axial rods to simulate roof structures at the head of walls. Thus, there are 157,480 elements in the entire model. Fig. 19 shows the generated FE model for the Cathedral.

4.2. First adjustment of mechanical properties

The first stage of model updating process was made by comparing the frequencies obtained experimentally (Table 1) with those calculated by the FE model, based on the initial parameter values

(Table 4). The match between modes for model updating is based on the visual qualitative assessment of the mode shapes (see Fig. 20) and quantification of the MAC between experimental mode shapes and those obtained from the numerical model (Table 5).

Given that the MAC will be used for comparing the analytical and experimental modes, the experimental modes require transformation to real values to compare them with the analytical ones. This transformation is important, because energy dissipation in a real structure cannot be represented by only viscous (proportional) damping, and therefore complex experimental modes are identified [19]. This is related to the presence of cracks in the structure and therefore the influence of these in the damping of the structure. The complexity of the experimental modes is then related to the presence of these cracks and gives us an idea of the current

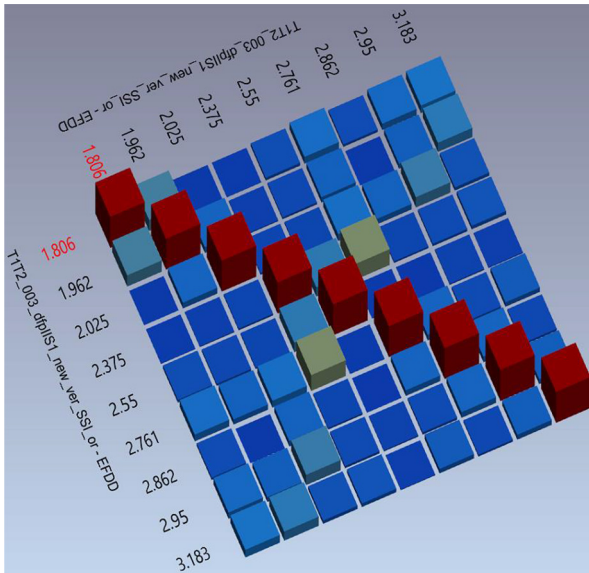


Fig. 18. MAC between experimental modes.

Table 1
Experimental frequencies.

Experimental mode	EFDD method Frequency (Hz)	SSI method Frequency (Hz)
1	1.81	1.74
2	1.96	1.93
3	2.03	2.06
4	2.38	2.38
5	2.55	2.56
6	2.76	2.79
7	2.86	2.86
8	2.95	2.93
9	3.18	3.20

Table 2
Results of Young's modulus and compressive strength obtained from monotonic compression testing of stone cylinders.

Specimen	$E_{30\%-60\%}$ (MPa)	f_c (MPa)
P1	13,400	115
P2	11,000	111
P3	17,200	109
Average values	13,900	111
Coef. of Variation	0.23	0.03

Table 3
Initial calibration parameter values.

Calibration parameter	Initial value
Young's modulus of stone masonry E_{sm} (MPa)	1390
Young's modulus of brick masonry E_{bm} (MPa)	1780
Young's modulus of the reinforced masonry E_{rm} (MPa)	1780
Lateral stiffness factor from Chapel	1.00
Lateral stiffness factor from Sacristy	1.00
Lateral stiffness factor from Tabernacle	1.00

damage of the structure. The comparison between these modes and the analytical modes was performed using the numerical transformation (Eq. (1)) purposed by Niedbal [37]:

$$\phi_{eX_R} = \text{Re}(\phi_{eX_C}) + \text{Im}(\phi_{eX_C})(\text{Re}(\phi_{eX_C})^T \text{Re}(\phi_{eX_C}))^{-1} \text{Re}(\phi_{eX_C})^T \text{Im}(\phi_{eX_C}) \quad (1)$$

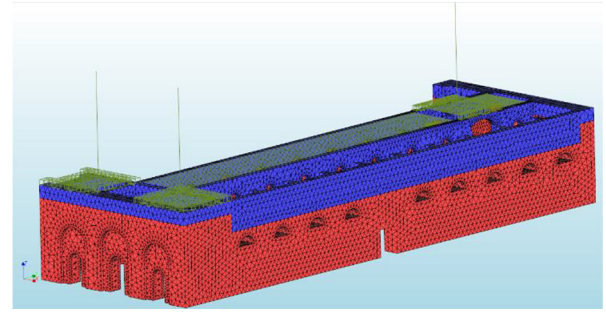


Fig. 19. FE model of the Cathedral.

Table 4
Numerical frequencies (initial calibration parameters).

Numerical mode	Frequency (Hz)	Mass participation based on FE model (%)	Mode description
1	1.38	0.48	Bending of south tower.
2	1.39	0.15	Bending of north tower.
3	1.41	0.61	Bending of south tower.
4	1.43	0.43	Bending of north tower.
5	1.90	27.48	Transverse bending of longitudinal walls.
6	2.02	0.27	Transverse bending of south longitudinal walls.
7	2.19	1.73	Transverse bending of longitudinal walls and bending dome.
8	2.27	0.11	Bending dome.
9	2.32	1.55	Transverse bending of longitudinal walls and bending dome.
10	2.40	0.53	Transverse bending of south longitudinal walls.
11	2.54	5.44	Bending dome.
12	2.56	0.02	Transverse bending of longitudinal walls.
13	2.59	0.63	Transverse bending of longitudinal walls.
14	2.83	2.24	Transverse bending of longitudinal walls.
15	2.97	0.22	Transverse bending of longitudinal walls.

where Re^* and Im^* are the real and imaginary parts of the complex mode, respectively; ϕ_{eX_C} and ϕ_{eX_R} are the experimental complex mode (obtained directly from the identification process) and the equivalent real mode, respectively. The lower limit value of MAC that was considered to be valid for this “modal equivalence” was 0.50. Some other studies (e.g. [42]) have started with MAC equal to 0.4 as the lower limit value.

Based on Table 4, the four first numerical modes were not considered, because they are related to towers movement, and the experimental model cannot reproduce this. It can be clearly seen in Tables 4 and 5 that 3 of the 4 selected modes have relatively large participation mass percentages. Note that in this type of structure, values accumulated from mass participation can only be achieved with many more modes than for conventional structures. Additionally, there are two important modes (modes 9 and 11) that have not been taken into account because these are related to dome movement.

As seen in Table 3, the calibration parameters considered for the model update were: (1) the Young's modulus of stone masonry; (2) the Young's modulus of brick masonry; (3) the Young's modulus of the reinforced masonry; (4) the lateral stiffness factor in the chapel support area; (5) the lateral stiffness factor in the tabernacle sup-

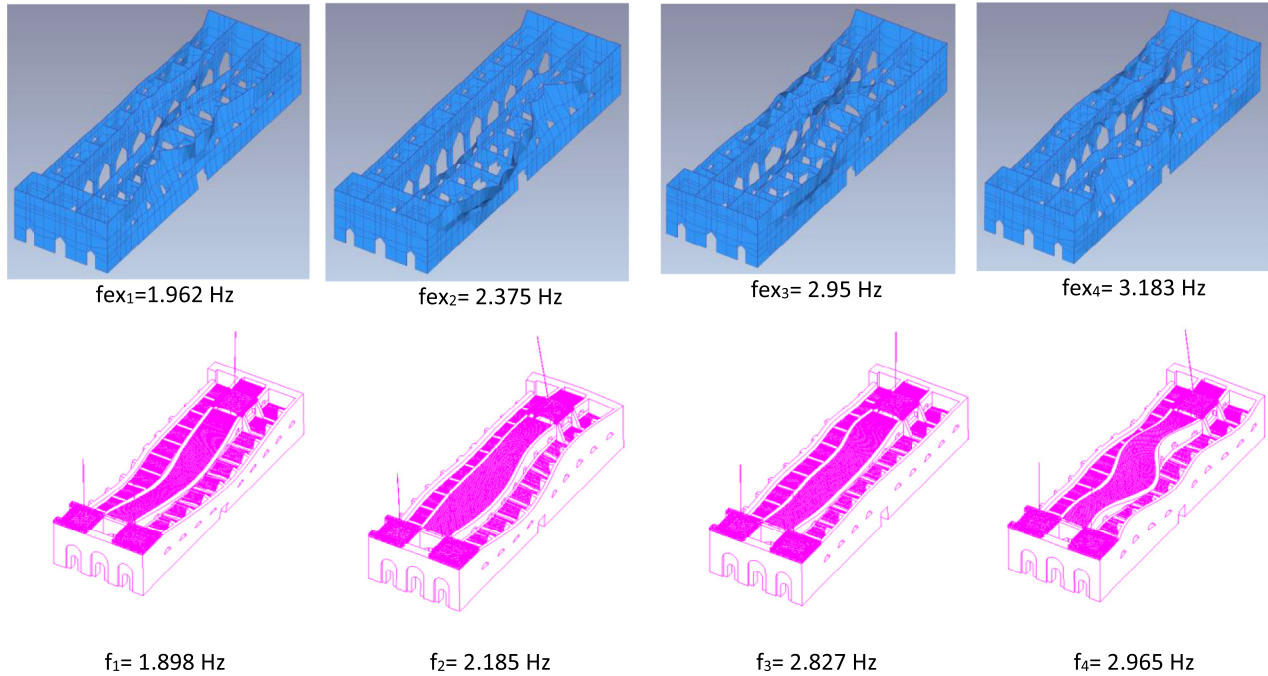


Fig. 20. Reference experimental modes and corresponding analytical global ones.

Table 5

Couples experimental and numerical (obtained with initial parameters) frequencies according to their similarity in modal shape and MAC.

Experimental Mode number	Experimental frequency (Hz)	Numerical Mode number	Numerical frequency (Hz)	MAC
2	1.96	5	1.90	0.85
4	2.38	7	2.19	0.61
8	2.95	14	2.83	0.55
9	3.18	15	2.97	0.69

port area; and (6) the lateral stiffness factor in the sacristy support area. These three last calibration parameters are dimensionless, because they are factors that multiply a vertical distribution of elastic supports in the zones where the principal structure is adjacent to before mentioned external structures. The vertical distribution of elastic supports has the following mean values per square meter: 472 MN/m for chapel, 2040 MN/m for tabernacle and 307 MN/m for sacristy. The initial values for these factors take unity values to begin the model updating. These calibration parameters have high uncertainty and influence in the model, so it is important to define their values in the model updating process. There are many other important calibration parameters that can participate in the model updating, like material mass, but their uncertainty is relatively low, as its identification was done in laboratory.

Various techniques have been proposed for updating models [19,27]. The method proposed by Douglas and Reid [14] was initially applied in this study.

The modal updating begins by defining an approximating function expressing the numerical frequency based on a quadratic function of the calibration parameters (Eq. (2)).

$$f_i = a_i x_j^2 + b_i x_j + c_i \quad (2)$$

where f_i represents the numerical frequency; a_i , b_i and c_i the quadratic function constants for each frequency, where i is the vibration mode; and x_j are the calibration parameters of the model, in this case $j = 1 \dots 6$. Then the error is defined as:

$$\varepsilon_i = f_i - f_{ex_i} \quad (3)$$

where f_{ex_i} is the corresponding experimental frequency.

This problem can now be treated as a multi-objective multivariable optimization problem, where each of the errors would be minimized. To simplify the problem, all error functions are concentrated in a single expression, and so the problem becomes a multi-variable optimization problem with a single objective, i.e. to optimize the function (Eq. (4)):

$$J = \sum w_i \varepsilon_i^2 \quad (4)$$

where w_i are the weights for each error, depending on the mode being evaluated. This weighting factor depends on the uncertainty associated with the experimental measurement, and the uncertainty associated with the numerical model [19]. Therefore, the expressions (2), (3) and (4) define the process for obtaining the error function that subsequently will be minimized in the first stage of model updating. The optimization process was performed based on the Karush-Kuhn-Tucker method using MATLAB Optimization [34].

As the dependence of the frequency on the parameters was assumed to be quadratic [14], 3 points needed to be defined on each parameter variation. The structure's natural frequencies were calculated when taking the minimum, maximum and nominal value for material parameters. The parameters were modified one at a time.

The nominal values for the parameters in the optimization process were: Young's modulus of stone masonry (E_{sm}) 1390 MPa (range of variation was from -15% to 40%), Young's modulus of brick masonry (E_{bm}) 1690 MPa (range of variation was from -25% to 5%), Young's modulus of the reinforced masonry (E_{rm}) 1870 MPa (range of variation was from -5% to 25%). Since the con-

tributed stiffness from adjacent structures does not have a single representative value, as they vary in height, the calculated value was multiplied by a factor of 1.00 and its variation was made based on this factor (range of variation was from -40% to 500%). After this function error minimization process, the calibration parameters were obtained (Table 6). These values are called frequency optimized values from now on.

4.3. Definition of models based on changing mechanical properties

The second stage of model updating was based on large number of models, generated in a grid search, in which the Young's modulus of materials vary within a defined range. The lateral stiffness factors do not change and the frequency optimized values were fixed.

A wider range of variation for the calibration parameters values was allowed (between 50% and approx. 150% of central values). Table 7 summarizes the central values (obtained from frequency optimization), minimum and maximum values for each parameter. The step increases in each parameter range were 10% but, when close to the central values, the increase was 5%. The total number of models generated with the described increments is 910.

Table 6
Frequency optimized values of calibration parameters with model updating based on function error minimization.

Calibration parameter	Frequency optimized value
Young's modulus of stone masonry E_{sm} (MPa)	1560
Young's modulus of brick masonry E_{bm} (MPa)	1700
Young's modulus of the reinforced masonry E_{rm} (MPa)	1870
Lateral stiffness factor from Chapel	3.265
Lateral stiffness factor from Sacristy	3.526
Lateral stiffness factor from Tabernacle	3.063

Table 7
Range of calibration parameters (910 models).

Calibration parameter	Min. value	Central value	Max. value
Young's modulus of stone masonry E_{sm} (MPa)	780	1560	2330
Young's modulus of brick masonry E_{bm} (MPa)	850	1700	2550
Young's modulus of the reinforced masonry E_{rm} (MPa)	940	1870	2810

The change of the calibration parameters is given by a multidimensional matrix where all possible combinations are given. The order of variation of the calibration parameters for exposition of the results in the next section is in cascade, starting with the variation of Young's modulus of the reinforced masonry, then the variation of Young's modulus of brick masonry, and finally the variation of Young's modulus of the stone masonry. The models for which Young's modulus of reinforced masonry was lower than for brick masonry were not included.

4.4. Model updating

The model updating process was done by comparing the modal parameters obtained experimentally with those calculated by FE model perturbation. The distance between models was calculated using expression (Eq. (5)).

$$d = \sum_{i=1}^M w_{i,MAC} \left[w_f \frac{|f_i - f_{ex_i}|}{f_{ex_i}} + w_\phi [1 - MAC(\phi_i, \phi_{ex_i})] \right] \quad (5)$$

where: f_i represents the numerical frequency, f_{ex_i} is the experimental frequency, ϕ_i represents the vector of the analytical modal shape, ϕ_{ex_i} is the vector of experimental modal shape, $w_{i,MAC}$ is the weighting factor based on the MAC between the analytical modal shape and experimental one, w_f is the weighting factor of frequency summation term and w_ϕ is the weighting factor of modal shape summation term; the last two weighting factors add up to unity. In all these terms, i subscript means mode that is being evaluated.

The expression (5) proposes that the frequency and modal shape have different weighting factors based on the confidence that exists in their experimental determination [19]. This expression relates all modes that participate in the model updating, distinguishing the different participation for frequency term against modal shape term, and additionally the different participation of each mode.

The value of the distance between the experimental model and each of the analytical models is plotted in Fig. 21. This figure shows a clear trend toward a minimum value in models with a Young's modulus of stone masonry between 1320 and 1630 MPa (model's number 300 to 500). In addition, the location of the model with nominal initial properties, and the model with frequency optimized values are shown. Even though the overall trend in Fig. 21a defines the existence of an optimum range of properties, focussing in on the area of interest (Fig. 21b) it shows that there is no unique representative minimum, from a practical point of view, since the trend of the curve is always monotonic when varying the Young's modulus of reinforced masonry.

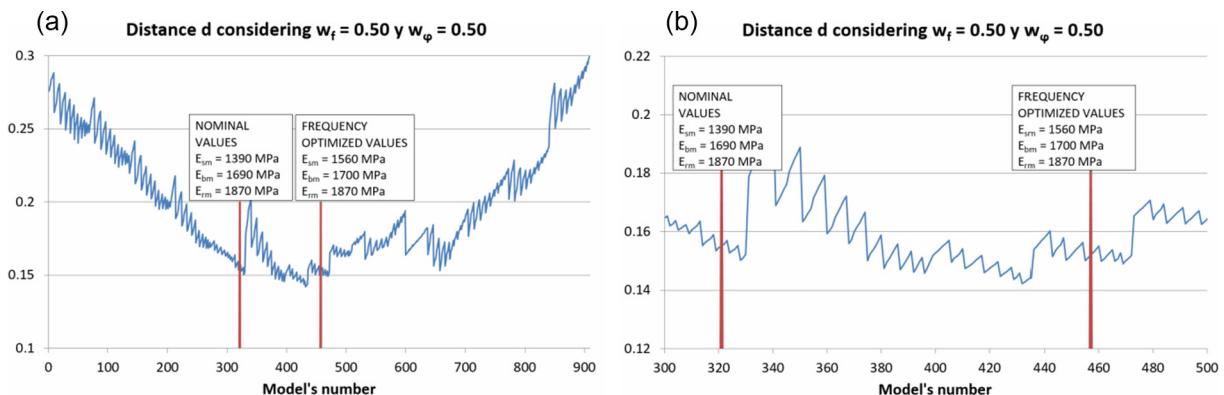


Fig. 21. Distance between analytical model and experimental model with the same participation for frequency and modal shape term, a) Distance for all models, b) Zoom into area of interest for Young's modulus of stone masonry between 1320 and 1630 MPa.

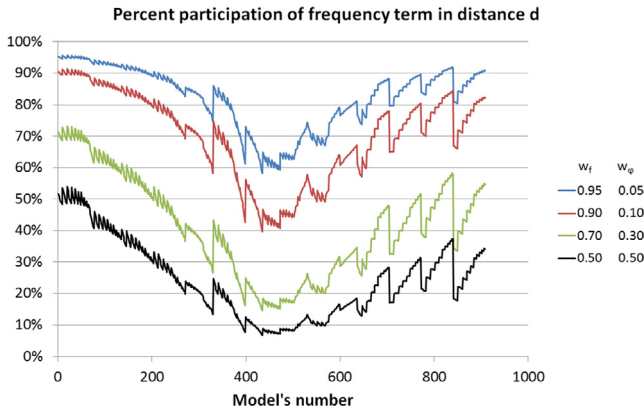


Fig. 22. Participation of frequency term in the distance value of expression (1) for different couples of weighting factors.

Several different weighting factors w_f and w_ϕ were tested to evaluate their effect on model selection, Fig. 22. This figure indicates that for the area of interest, located between the models with a Young’s modulus of stone masonry between 1400 and 1720 MPa (model’s number 350 and 600) approximately, the frequency participation is not similar to the weighting factors entered. It is noted that for the case where the two terms weigh the same (each 50%), the frequency term has a 10% of participation in the distance value and correspondingly the modal shape term would present a 90% of participation within the area of interest. For the case in which the weighting factor in the frequency term is 0.70, its participation reaches approximately 20% of the distance. For the case in which the weighting factor of the frequency term is 0.90, its participation is 50% of the distance. Finally, just when it has a weighting factor of 0.95 of the frequency term, its participation is about 65% of the distance. It is only in the latter case when the recommendation in the literature is fulfilled. We therefore chose to work with these 3 last cases (0.70–0.30, 0.90–0.10 and 0.95–0.05 for w_f and w_ϕ respectively) and to evaluate their results (Fig. 23). In Fig. 23 there are some marks (models with specific values for calibration parameters) named as “minimum values to analyze”. These models will be reviewed in the next section.

5. Results of model updating

Two reference values were defined to continue evaluating the appropriate values for calibration parameters: errors between frequencies and the MAC, both between the experimental and the analytical model (Table 8). The analytical model was performed based on frequency optimized values (Table 6).

Table 9 shows the average error frequency and mean change for MAC in each model. The difference between the experimental and analytical frequency should be as low as possible; for the modal shape, MAC change between the analytical model with frequency optimized values and the experimental model should be positive. Thus, the analytical models 446, 451, 458 and 464 (in bold and gray background) are closest to the experimental model in the case $w_f = 0.90$ and $w_\phi = 0.10$.

A new variation range for the calibration parameters was therefore defined for the new area of interest (Table 10), where the steps of variation were 3%. The additional number of models generated for this last step is 147. The order for arranging these models based on changing parameters follows the same logic as the 910 previously analyzed models. The calculated distance for this group of models can be seen in Fig. 24.

Given the short difference between the experimental and analytical models (between 0.045 and 0.055) for this new group (see

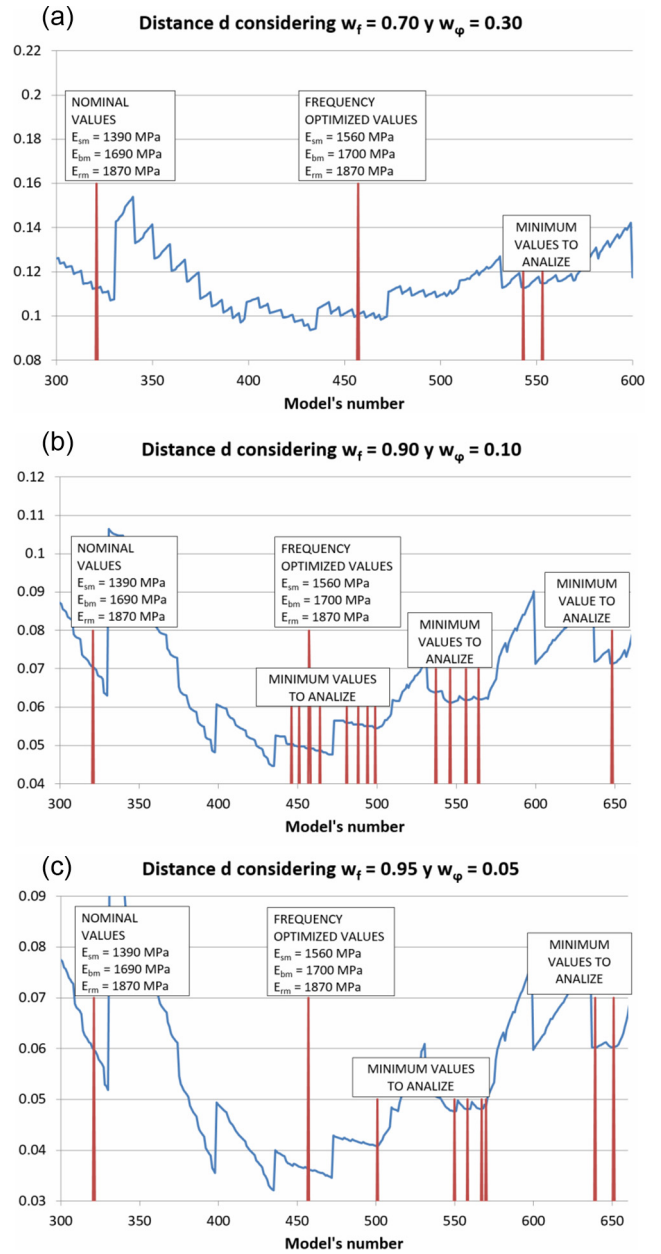


Fig. 23. Distance between analytical and experimental model – for cases in which the factors w_f and w_ϕ vary. a) Case 1. Zoom in area of interest for Young’s modulus of stone masonry between 1400 and 1720 MPa. b) Case 2. Zoom into area of interest for Young’s modulus of stone masonry between 1320 and 1870 MPa. c) Case 3. Zoom in area of interest for Young’s modulus of stone masonry between 1320 and 1870 MPa.

Fig. 24), they will no longer be analyzed based on whether or not they have a strict minimum value, but rather by evaluating directly the error between experimental and analytical frequencies, and the MAC variation between the analytical and experimental modal shapes in the corresponding mode.

The error regarding the experimental frequency of each mode is represented in Fig. 25. The analytical model is appropriate when the frequency error is below the segmented lines; these lines indicate the reference limits generated by the analytical frequency error, based on the analytical model with frequency optimized values.

Fig. 26 uses the MAC analysis between each pair of analytical and experimental modal shapes. The MAC value in this figure is plotted and compared with the MAC for the analytical model with

Table 8
Reference values for frequencies and modal shapes.

	Mode 1	Mode 2	Mode 3	Mode 4
Experimental frequencies (Hz)	1.96	2.38	2.95	3.18
Analytical frequencies for frequency optimized values (Hz)	2.00	2.28	2.97	3.11
Percentage errors between frequencies	2.0%	4.2%	0.8%	2.4%
MAC	0.85	0.64	0.59	0.74

Table 9
Analysis of frequencies and modal shapes for models with valid minimum distances.

Weighting factors		Model's number	Values of calibration parameters			Analytical frequencies (Hz) with percentage errors					MAC with percentage changes						
w_f	w_ϕ		E_{sm} (MPa)	E_{bm} (MPa)	E_{rm} (MPa)	Mode 1	Mode 2	Mode 3	Mode 4	avg. error	Mode 1	Mode 2	Mode 3	Mode 4	avg. change		
0.70	0.30	543	1716	1020	1122	2.06	2.26	2.97	3.05		0.85	0.15	0.55	0.77			
						5.0%	4.6%	0.6%	4.1%	3.6%	0.3%	-76.4%	-6.7%	4.3%	-19.6%		
0.90	0.10	446	1555	1528	1960	2.00	2.27	2.95	3.08		0.85	0.61	0.58	0.74			
						1.8%	4.6%	0.0%	3.2%	2.4%	-0.1%	-4.3%	-1.1%	0.1%	-1.4%		
		451	1555	1613	1867	2.00	2.27	2.96	3.09		0.85	0.63	0.59	0.74			
						1.9%	4.4%	0.4%	2.8%	2.4%	0.0%	-1.7%	-0.3%	0.4%	-0.4%		
		458	1555	1698	1961	2.00	2.28	2.97	3.11		0.85	0.63	0.59	0.74			
						2.1%	4.2%	0.8%	2.3%	2.3%	0.0%	-1.2%	0.0%	-0.1%	-0.3%		
		464	1555	1783	2054	2.01	2.28	2.98	3.13		0.85	0.64	0.59	0.74			
						2.2%	4.0%	1.2%	1.7%	2.3%	-0.1%	-0.8%	0.3%	-0.7%	-0.3%		
		481	1632	1528	1774	2.04	2.29	3.01	3.13		0.85	0.48	0.59	0.75			
						4.1%	3.6%	1.9%	1.7%	2.8%	0.0%	-25.7%	-0.4%	1.1%	-6.2%		
		0.95	0.05	501	1632	1783	2054	2.05	2.30	3.04	3.18		0.85	0.50	0.59	0.74	
								4.6%	3.0%	3.1%	0.0%	2.7%	-0.1%	-22.5%	0.7%	-0.3%	-5.6%

Table 10
Range of calibration parameters in interest zone (147 models).

Calibration parameter	Min. value	Central value	Max. value
Young's modulus of stone masonry E_{sm} (MPa)	1510	1550	1600
Young's modulus of brick masonry E_{bm} (MPa)	1540	1700	1850
Young's modulus of the reinforced masonry E_{rm} (MPa)	1780	1960	2140

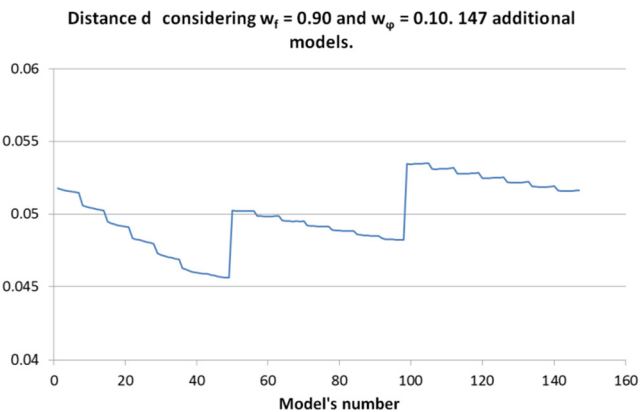


Fig. 24. Distance between analytical and experimental model – Second stage.

Variation of frequency error (%) in range of minimum valid values

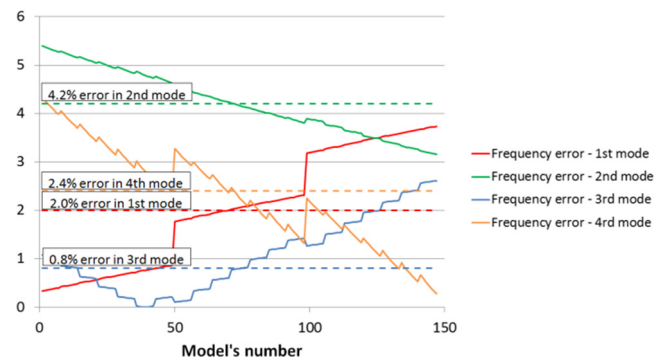


Fig. 25. Frequency error for each mode.

frequency optimized values (segmented lines) as a reference. The analytical model is appropriate when the MAC values are above the segmented lines.

Analyzing Figs. 25 and 26, the first two sections of the elasticity modulus variation for stone masonry is an appropriate range when the MAC is adequate; however, this conclusion would only be true for the frequency error for the first and third mode. As the frequency error variation is not large, the sections mentioned in the elasticity modulus for stone can be said to be adequate; the other two modules can vary within the full range defined in this new

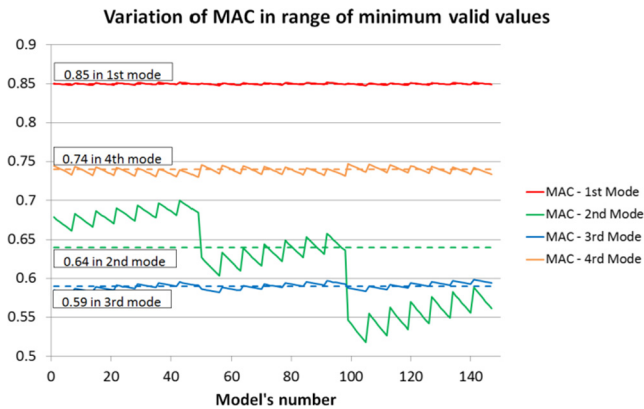


Fig. 26. MAC for each mode.

Table 11

Valid ranges of calibration parameters.

Calibration parameter	Min. value	Max. value
Young's modulus of stone masonry E_{sm} (MPa)	1510	1550
Young's modulus of brick masonry E_{bm} (MPa)	1540	1850
Young's modulus of the reinforced masonry E_{rm} (MPa)	1780	2140

variation of the 147 models (Table 10). Therefore, adequate ranges of calibration parameters can be established that get an analytical model similar to experimental one, based on in situ measurements. These ranges are shown in Table 11.

Fig. 27 graphically indicates the closeness of experimental frequencies and modal shapes with analytical frequencies. This graphs are similar to FMAC (Frequency-scaled MAC) [16], and concentrate all the information on error frequencies and MAC between experimental and analytical modes in one picture. These graphs show FMAC for comparing calibration parameters that were assumed as frequency optimized values, and the results of second stage. These cases correspond to analytical models with minimum and maximum values indicated in Table 11. The size of the circles shown relates to the MAC in the analytical and experimental modes. It should be noted that the optimal ranges obtained for the calibration parameters produce adequate results in both frequencies and mode shapes through MAC.

6. Brief discussion and suggestions

The structure's natural frequencies concentrate to a narrow band; there are 4 experimental frequencies considered to the model updating in the 1.90 to 2.97 Hz range, and all these considered modes correspond to the out-of-plane flexure of the longitudinal walls. The first stage of the model updating process obtained similar results to the second one. Despite this, the latter takes into account the comparison between modal shapes by calculating the MAC between experimental and analytical modes.

As mentioned before, the selection of the calibration parameters involved in model updating depends on the importance of the variable in the model and the uncertainty that exists in its determination. In the first stage, the elastic moduli of the materials and the stiffness factors of the interaction conditions of the adjacent structures were defined as calibration parameters, only the modulus of elasticity was varied for the second stage since each new parameter increases by an order of magnitude the number of models to analyze.

The model updating stages determine single values (first stage) or physically possible ranges for calibration parameters (second stage). This processes contain uncertainties related with: the modeling of the structure, uniformity of mechanical properties in materials, noise present in measuring structure response to ambient vibration, the interaction between plane resistant components of the structure, among others. These uncertainties, although not explicitly considered in the model updating, are responsible for additional changes in the final obtained ranges of calibration parameters. The second stage of model updating process has shown that the range of values for each calibration parameter is best suited to representing the current behavior of the Metropolitan Cathedral of Santiago Chile in future research. The final frequency errors show for both stages that the presented results are adequate, because the major error was not more than 5%, and the MAC values were maintained at approximately the same value between the both stages.

The Young's modulus of stone masonry is the most important value for the model updating. All graphs that show the distance between experimental and analytical models have stronger changes in the variation of this calibration parameter. Future research can be developed by considering the fact that the Cathedral is made up of single material (stone masonry) and assessing how different the results could be with this new consideration. This option is very important because if the number of calibration parameters is reduced, the workload will decrease, and other parameters can be considered, like stiffness factors in all support conditions.

Based on the experience gained during the research, some suggestions can be done in order to help future studies or engineering projects:

- The referential sensors must be located in places of the structure where movement is important for most modes. For that, a numerical model should be developed before the experimental campaign. The other sensors should be successively distributed based on the modes the user wants to capture. Other factors to consider in the experimental campaign are: measurement time, synchronizing the sensors and their precision.
- It is important to validate the records after each measurement. For that, the synchronization of sensors must be check in each setup. This can be done based on the graph of phase angle for transfer functions between measurements of the same setup.
- Evaluate the tool for identifying the system to be used. This tool can be generated by the user, or can be a commercial software built for this purpose. Similarly, the user should plan the tool for model updating. All these tools should be validated to ensure good performance in the study.
- If one of the calibration parameters is more important than the others in the final results, this fact should be properly evaluated, because the model updating could solely focus on this parameter. The model updating based on the second stage proposed in this study could be developed more quickly, with fewer calibration parameters, or it can neglect certain parameters to take others into account.
- The researcher experience is very important, because there are many decisions that are based on good judgment. All definitions in the process should be supported with alternative methods or literature related to the subject.
- In the case of study of model updating of structure based on local modes, it is important to note the process to follow in the experimental campaign. Firstly, the analytical model must be developed for defining the structure sensor locations. Secondly, the experimental campaign should be done, if the system identification process suggests the presence of local modes, it is important to update the analytical model so that these modes

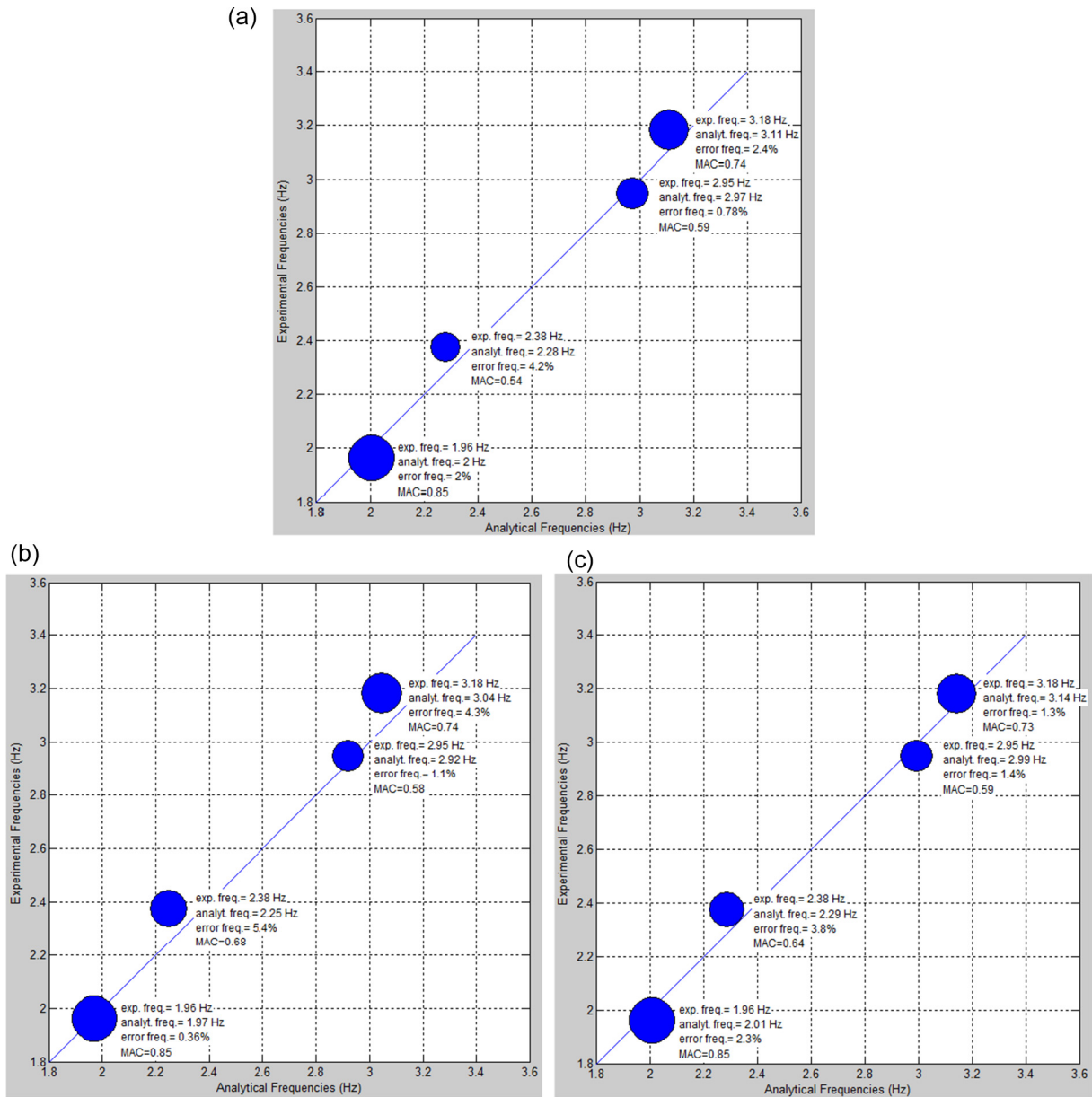


Fig. 27. Graphical comparison between analytical and experimental frequencies for many cases: a) Frequency optimized values of calibration parameters, b) Minimum values in calibration parameters of final ranges, c) Maximum values in calibration parameters of final ranges.

can be observed in the model. Finally, new setups must be planned to obtain information about these experimental local modes, which will be the basis for the final model updating.

7. Conclusions

This research presents the system identification of Cathedral of Santiago Chile in two stages. The first stage is the traditional method, based on minimizing an error function, and the other is based on simulation of many models that varied the Young's modulus of structural materials. Single values for each parameter was obtained from the first stage; these values are physically logical because they are inside the initially proposed range. By contrast, the second stage produces a physical range for each calibration parameter, which was a harder process but with a major interaction by the user. From this research, the following conclusions can be drawn:

The experimental campaign, carried out through in-situ dynamic testing, was one of the better ways of studying this structure. The information obtained about the material properties was very valuable, because this is a necessary input for future research into the structure's seismic performance. Additionally, OMA tests, with their non-invasive characteristics, allowed for the study of the structure without affectation and in service. Therefore, based on a non-destructive technique, the bases of a study related with the safe of this important structure can be defined.

The numerical model has been considered with all nodes rigidly joined; additionally, the experimental model, generated with the participation of all setups, has meant that global modes were used in the study of the structure. It is important to note that if the researcher wants to see the local modes, both the numerical and experimental model should be planned accordingly. This is an opportunity for further study i.e. the model updating of the structure based on local modes.

In the distance formulae for evaluating the similarity between experimental and analytical models, the term related to the modal shapes did not strongly change in the series of analyzed models; this is because the calibration parameters were only Young's modulus of materials in the second stage; it probably would produce a better result if there were many more calibration parameters related to the structure support.

Determining ranges in the model calibration parameters depends on weighting factors; the models show the local minimum, as referenced in the graphs of this paper, only when the weighting factors have certain values aligned with the confidence of their determination, specifically the frequency term and modal shape term in the distance formulae.

The two stages of model updating produced similar results. The first stage obtains a single value for each calibration parameter, while the second allows to get ranges of values for each parameter. This latter can be more consistent with the structure's reality, because it is physically more logical to have a valid range for each calibration parameter, given the variability in structure properties. Additionally, in the second stage, the whole process is carried out based on logical steps given by the physics of the problem, while the first stage has a mathematical foundation that minimizes researcher judgment in solving the problem.

Although the results between stages are very close, it is important to note that the computational cost of the second stage is much greater; a practical definition would then be that the first stage is enough to get adequate results. However, although there is no greater difference between the results of these stages, there is a greater certainty in obtaining the results in the second stage because the interaction achieved by the user with the adjustment of the model is much greater.

Acknowledgments

The first author acknowledges the support of the Secretary of Higher Education, Science, Technology and Innovation of Ecuador (SENESCYT), through contract number 20120011. The authors acknowledge the support of the researcher Fernando Pérez, through FONDECYT project number 1110481, and Professor Pablo Gonzalez of Universidad Diego Portales for the loan of TROMINOS. Finally, special thanks are owed to the group of graduate students from the Catholic University of Chile in 2014, and group of DICTUC workers who helped in the experimental campaign measurement of the Cathedral's ambient vibrations.

References

- [1] Aguilar R, Marques R, Sovero K, Martel C, Trujillano F, Boroschek R. Investigations on the structural behaviour of archaeological heritage in Peru: From survey to seismic assessment. *Engineering Structures* 2015;95:94–111.
- [2] Allemang, R. J., & Brown, D. L. (1982). A correlation coefficient for modal vector analysis. In *International Modal Analysis Conference* (pp. 110–116).
- [3] Aras F, Krstevska L, Altay G, Tashkov L. Experimental and numerical modal analyses of a historical masonry palace. *Construction and Building Materials* 2011;25(1):81–91.
- [4] Bayraktar A, Altunışık AC, Sevim B, Türker T, Akköse M, Çoşkun N. Modal analysis, experimental validation, and calibration of a historical masonry minaret. *Journal of Testing and Evaluation* 2008;36(6):516–24.
- [5] Binda, L., & Saisi, A. (2009). Knowledge of the building, on site investigation and connected problems. Eurocode 8 Perspectives from the Italian Standpoint Workshop, Napoli, 213–224.
- [6] Brincker, R., Ventura, C. E., & Andersen, P. (2001). Damping Estimation by Frequency Domain Decomposition. In *19th International Seminar on Modal Analysis* (pp. 698–703).
- [7] Brincker, R., Zhang, L., & Andersen, P. (2000). Modal identification from ambient responses using Frequency Domain Decomposition. In *18th International Seminar on Modal Analysis*.
- [8] Cabboi, A., Magalhães, F., Gentile, C., & Cunha, Á. (2013). Automatic operational modal analysis: Challenges and practical application to a historical bridge. *Eccomas Conference on Smart Structures and Materials*, (June), 24–26.
- [9] Carpinteri A, Invernizzi S, Lacidogna G. In situ damage assessment and nonlinear modelling of a historical masonry tower. *Engineering Structures* 2005;27(3):387–95.
- [10] Caselles O, Martínez G, Clapes J, Roca P, Pérez MDLV. Application of particle motion technique to structural modal identification of heritage buildings. *International Journal of Architectural Heritage* 2013;9:310–23.
- [11] CIMNE. (2014). GiD. Retrieved from [ftp://www.gidhome.com/pub/GiD_Documentation/Docs/GiD_Reference_Manual.pdf](http://www.gidhome.com/pub/GiD_Documentation/Docs/GiD_Reference_Manual.pdf).
- [12] De Stefano A, Ceravolo R. Assessing the health state of ancient structures: The role of vibrational tests. *Journal of Intelligent Material Systems and Structures* 2007;18(8):793–807.
- [13] Doebling S, Farrar CR, Prime M. A summary review of vibration-based damage identification methods. *The Shock and Vibration Digest* 1998;30:91–105.
- [14] Douglas B, Reid W. Dynamic test and system identification of bridges. *Journal of the Structural Division* 1982;108:2295–312.
- [15] Elyamani A, Caselles O, Roca P, Clapes J. Dynamic investigation of a large historical cathedral. *Structural Control and Health Monitoring* 2016;24(3):e1885.
- [16] Ewins D. *Modal testing theory, practice and application* (John Wiley & Sons Ltd., Ed.). Second ed. Research Studies Press Ltd.; 2000. pp. 433–434.
- [17] Feenstra PH, De Borst R. A composite plasticity concrete model for concrete. *International Journal of Solids and Structures* 1996;33(5):707–30.
- [18] Foti D, Diaferio M, Giannocaro NI, Mongelli M. Ambient vibration testing, dynamic identification and model updating of a historic tower. *NDT and E International* 2012;47:88–95.
- [19] Friswell M, Mottershead J. *Finite element model updating in structural dynamics*. The Netherlands, Dordrecht: Kluwer Academic; 1995.
- [20] Gentile C, Saisi A. Ambient vibration testing of historic masonry towers for structural identification and damage assessment. *Construction and Building Materials* 2007;21(6):1311–21.
- [21] Gentile Carmelo, Saisi A, Cabboi A. Structural identification of a masonry tower based on operational modal analysis. *International Journal of Architectural Heritage* 2015;9(2):98–110.
- [22] Goodman R. *Introduction to Rock Mechanics* (John Wiley & Sons, Ed.). Second ed, 1989.
- [23] Goursat, M., Dohler, M., Mevel, L., & Andersen, P. (2010). Crystal Clear SSI for Operational Modal Analysis of Aerospace Vehicles. In *Proceedings of the 28th International Modal Analysis Conference (IMAC)*, Jacksonville, Florida.
- [24] IDIEM. (2011). Estudio de ingeniería estructural edificio Catedral Metropolitana. Santiago de Chile.
- [25] ISCARSAH (International Scientific Committee for Analysis and Restoration of Structures of Architectural Heritage). Recommendations for the analysis, conservation and structural restoration of Architectural Heritage. *ICOMOS*; 2003. pp. 3–6.
- [26] Italian Code for Constructions NTC08. (2008). Norme tecniche per le costruzioni (NTC 2008) - Decreto 14 gennaio. Supplemento ordinario alla G. U. n. 29 del 4 febbraio 2008 - in Italian. 2008.
- [27] Kim G-H, Park Y-S. An improved updating parameter selection method and finite element model update using multiobjective optimisation technique. *Mechanical Systems and Signal Processing* 2004;18(1):59–78.
- [28] Leyton F, Ruiz S, Sepúlveda S. Reevaluación del peligro sísmico probabilístico en Chile central. *Andean Geology* 2010;37(2):455–72.
- [29] Lorenzoni F, Casarin F, Modena C, Caldón M, Islami K, da Porto F. Structural health monitoring of the Roman Arena of Verona, Italy. *Journal of Civil Structural Health Monitoring* 2013;3(4):227–46.
- [30] Lourenço P. Computational strategies for masonry structures PhD Thesis. The Netherlands: Delft University of Technology; 1996.
- [31] Lourenço PB, Krakowiak KJ, Fernandes FM, Ramos LF. Failure analysis of Monastery of Jerónimos, Lisbon: How to learn from sophisticated numerical models. *Engineering Failure Analysis* 2007;14(2):280–300.
- [32] Masciotta M-G, Roque JCA, Ramos LF, Lourenço PB. A multidisciplinary approach to assess the health state of heritage structures: The case study of the Church of Monastery of Jerónimos in Lisbon. *Construction and Building Materials* 2016;116:169–87.
- [33] Masjedian, M., & Keshmiri, M. (2009). A Review on Operational Modal Analysis Researches : Classification of Methods and Applications. In *IOMAC'09 - 3rd International Operational Modal Analysis Conference* (pp. 707–716).
- [34] Mathworks. (2015). MATLAB.
- [35] Meli, R. (1998). *Ingeniería Estructural de los Edificios Históricos*. (Fundación ICA. A.C., Ed.) (Primera ed.). México D.F.
- [36] MICROMED. (2012). User's manual.
- [37] Nield, N. (1984). Analytical determination of real normal modes from measured complex responses. Paper presented at the *Collection of Technical Papers - AIAA/ASME/ASCE/AHS/ASC Structures, Structural Dynamics and Materials Conference*, (pt 2) 292–295.
- [38] Oliveira D. Experimental and numerical analysis of blocky masonry structures under cyclic loading PhD Thesis. Guimaraes, Portugal: Universidade do Minho; 2002.
- [39] Page A. Finite element model for brick masonry. *Journal of Structural Division ASCE* 1978;104:1267–85.
- [40] Pérez, F., Beas, M., Leonard, D., Muzio, F., Pardo, J., & Prado, F. (2009). El interior de la Catedral: antecedentes histórico morfológicos y bases para su conservación. Santiago de Chile.
- [41] Prado C, Barrientos M. Aporte de la arqueología al estudio urbano de la ciudad de Santiago de Chile. El caso de "la manzana de la catedral". *Canto Rodado* 2011;6:1–32.

- [42] Ramos L, Aguilar R, Lourenço P, Moreira S. Dynamic structural health monitoring of Saint Torcato church. *Mechanical Systems and Signal Processing* 2013;35(1–2):1–15.
- [43] Ramos LF, Marques L, Lourenço PB, De Roeck G, Campos-Costa A, Roque J. Monitoring historical masonry structures with operational modal analysis: Two case studies. *Mechanical Systems and Signal Processing* 2010;24(5):1291–305.
- [44] Roca P, Cervera M, Gariup G, Pelà L. Structural analysis of masonry historical constructions. Classical and advanced approaches. *Archives of Computational Methods in Engineering* 2010;17(3):299–325.
- [45] Rodriguez J. Identificacao Modal Estocástica, Métodos de Análise e Aplicacoes em Estruturas de Engenharia Civil PhD Thesis. Porto, Portugal: University of Porto; 2004.
- [46] Structural Vibration Solutions A / S. (2015). ARTeMIS.
- [47] Diana TNO. DIANA finite element analysis. Delft: TNO Diana; 2015.
- [48] Torres, W., Almazán, J. L., Sandoval, C., & Boroschek, R. (2016). Determination of modal properties and FE model updating of the Metropolitan Cathedral of Santiago de Chile. In 10th Structural Analysis of Historical Constructions: Anamnesis, diagnosis, therapy, controls (pp. 804–811).
- [49] Valenzuela, G. (1978). Suelo de Fundacion del Gran Santiago.
- [50] Valledor, R., López-García, D., & Sandoval, C. (2015). Linearly elastic seismic evaluation of masonry historical buildings in Santiago, Chile: The case of the Pereira Palace. In 3rd International Conference on Mechanical Models in Structural Engineering, Sevilla, Spain.
- [51] Van Overschee P, De Moor B. Subspace identification for linear systems. theory – implementation – applications. (K. U. Leuven, Ed.) (First.). Leuven: Kluwer Academic Publishers; 1996.